A new method for estimating UV fluxes at ground level in cloud-free conditions

William Wandji Nyamsi[1,2], Mikko R. A. Pitkänen[2,3], Youva Aoun[1], Philippe Blanc[1], Anu Heikkilä[4], Kaisa Lakkala[4, 5], Germar Bernhard[6], Tapani Koskela[7], Anders V. Lindfors[2], Antti Arola[2] and Lucien Wald[1]

[1]MINES ParisTech, PSL Research University, Centre Observation, Impacts, Energy, Sophia Antipolis, France
[2]Finnish Meteorological Institute, Kuopio, Finland
[3]Department of Applied Physics, University of Eastern Finland, Kuopio, Finland
[4]Finnish Meteorological Institute, Climate Research, Helsinki, Finland
[5]Finnish Meteorological Institute, Arctic Research, Sodankylä, Finland
[6]Biospherical Instruments Inc., San Diego, California, USA
[7]Independent researcher, Helsinki, Finland

Correspondence to: William Wandji Nyamsi (william.wandji@fmi.fi)

Abstract. A new method has been developed to estimate the global and direct solar irradiance in the UV-A and UV-B, at ground level in cloud-free conditions. It is based on a resampling technique applied to the results of the *k*-distribution method and the correlated-*k* approximation of Kato et al. (1999) over the UV band. Its inputs are the aerosol properties, and total column ozone that are produced by the Copernicus Atmosphere Monitoring Service (CAMS). The estimates from this new method have been compared to instantaneous measurements of global UV irradiances made in cloud-free conditions at five stations at high latitudes in various climates. For the UV-A irradiance, the bias ranges between -0.8 W m^{-2} (-3% of the mean of all data) and -0.2 W m^{-2} (-1%). The root mean square error (RMSE) ranges from 1.1 W m^{-2} (6%) to 1.9 W m^{-2} (9%). The coefficient of determination R^2 is greater than 0.98. The bias for UV-B is between -0.04 W m^{-2} (-4%) and 0.08 W m^{-2} (+13%) and the RMSE is 0.1 W m^{-2} (between 12% and 18%). R^2 ranges between 0.97 and 0.99. This work demonstrates the quality of the proposed method combined with the CAMS products. Improvements, especially in the modelling of the reflectivity of the Earth's surface in the UV region, are necessary prior its inclusion into an operational tool.

1. Introduction

Solar ultraviolet (UV) radiation at the Earth's surface has beneficial and adverse effects on human health (Juzeniene et al., 2011). For instance, UV radiation is a principal source of vitamin-D, while the excess UV exposure is a risk factor for skin cancers, cataracts and immunosuppression. The wavelength dependence of these effects is typically characterized by action spectra. The most widely used one is the standardized action spectrum for erythema, also known as the CIE (Commission Internationale de l'Eclairage) spectrum (McKinlay and Diffey, 1987). There are also other action spectra related to skin cancer and melanoma (de Gruijl et al., 1993; Setlow et al., 1993). Emphasis has been put mostly on the assessment of the solar UV-erythemal irradiance, also known as the UV-CIE, and the derived quantity, the UV index, a very popular quantity to inform the public about UV levels. The UV index is also used in campaigns promoting safe sun exposure. While the UV-B [280, 320] nm band is the major contributor to UV-CIE, interest is growing in the role of UV-A [320, 400] nm and UV [280, 400] nm on various diseases, such as viral infections (Norval, 2006), multiple sclerosis (Orton et al., 2011), Parkinson disease (Kravietz et al., 2017), eye diseases (Delcourt et al., 2014), skin cancer (Coste et al., 2015; Fortes et al., 2016), or thyroid cancer (Mesrine et al., 2017), among many others (Juzeniene et al., 2011; Norval and Halliday, 2011).

Ground-based spectroradiometers are one of the means to monitor the intensity of solar UV fluxes. Such measurements are rare due to high costs of the instruments, operations and maintenance. To overcome this scarcity, many researchers have looked for proxies and have studied the relationship between UV radiation and the surface downwelling solar radiation integrated from 280 nm to 2800 nm), called broadband radiation, since the latter is measured at a greater number of stations or can be estimated at any place from satellite images (Blanc et al., 2011; Lefèvre et al., 2014). Several empirical relationships have been published that relate, with the knowledge of the total ozone column (TOC), the broadband irradiance to the UV-CIE (den Outer et al., 2010; Calbo et al., 2005) or the UV-A, UV-B or UV irradiance (Aculinin et al., 2016; Canada et al., 2003; Foyo-Moreno et al, 1998).

An alternative way is the use of an appropriate radiative transfer model (RTM) together with accurate inputs describing the state of the atmosphere in cloud-free condition and the properties of the ground surrounding the instrument. libRadtran is such a RTM (Emde et al., 2016; Mayer and Kylling, 2005). A comparison between 1200 measured UV spectra and estimates made

with a previous version called uvspec —now part of libRadtran— with only ozone and aerosol optical properties as inputs yielded very good performance to simulate the UV irradiance under cloud-free conditions (Mayer et al., 1997). The relative biases ranged between -11% and +2% for wavelengths between 295 nm and 400 nm and solar zenithal angles (SZA) up to 80°. Using measurements from sites in Finland, Norway and Sweden, Lindfors et al. (2007, 2009) showed that UV-CIE and spectral UV irradiances can be accurately modelled using libRadtran and broadband radiation, TOC, the total water vapor column from the ERA-40 data set, the surface albedo as estimated from snow depth, and the altitude of the location as input.

RTMs are usually computationally expensive; about hundreds of spectral calculations are required to compute the UV irradiance in a RTM. Strategies have been built to reduce the amount of calculations. Among them, are the *k*-distribution method and correlated-*k* approximation by Kato et al. (1999). The approach was originally designed for the calculation of the broadband solar irradiance. It consists in calculating the total solar irradiance, i.e. integrated between 240 nm to 4000 nm, with only 32 spectral calculations in the spectral range between 240 nm and 4606 nm. The operational McClear model estimating the total irradiance in cloud-free conditions accurately reproduces the irradiance computed by libRadtran based on the Kato et al. approach (Lefèvre et al.; 2013). The McClear model uses several abaci computed by libRadtran for selected values of inputs and provides irradiance at each of 32 spectral intervals. Hereafter, these 32 spectral intervals are named Kato bands and abbreviated KB with the number in subscript. Four KB are covering the whole UV range: KB_3 [283, 307] nm, KB_4 [307, 328] nm, KB_5 [328, 363] nm and KB_6 [363, 408] nm. In KB_1 and KB_2, atmospheric ozone attenuates the radiation before it reaches the ground.

Wandji Nyamsi et al. (2014) compared atmospheric transmissivities obtained by the Kato et al. approach against those obtained by spectrally resolved computations using two RTMs in each of the 32 KBs. These calculations were performed for a set of 200,000 realistic atmospheres and clouds. As for the UV band, the authors found that the Kato et al. approach offers very accurate estimates of irradiances in KB_5 and KB_6. On the contrary, a very large underestimation of the transmissivity was observed in KB_3 [283, 307] nm and KB_4 [307, 328] nm by respectively -93% and -16% in relative value and exhibits relative root mean square error of 123% and 17% in clear-sky conditions. Similar relative errors are observed for cloudy conditions. This is due to the assumption made by Kato et al. (1999) that in these bands, a single ozone cross section at the central wavelength is sufficient to accurately represent the

3

absorption by ozone over the whole interval. In a subsequent work, Wandji Nyamsi et al. (2015b) have proposed a novel parameterization using more than one single ozone cross sections which accurately represents the transmissivity due to ozone absorption. The novel parameterization of the transmissivity using more quadrature points yields maximum error of respectively 0.0006 and 0.0143 for intervals KB_3 and KB_4. Version 2.0.1 of libRadtran (Emde et al., 2016) includes this correction and has been used in this study.

The KBs do not fit exactly the UV spectral ranges and a spectral resampling is necessary. This is the subject of the present article. The concept of the novel method is to determine several 1-nm spectral bands whose atmospheric transmissivities are correlated to those of the KB and then use these transmissivities in a linear interpolation process to compute the UV irradiance. The method is empirically implemented by the means of libRadtran in cloud-free conditions. The concept has already been tested for photosynthetically active radiation (PAR) simulated by libRadtran (Wandji Nyamsi et al., 2015a). Now, the concept is tested for actual UV fluxes. This work is part of a larger project whose overarching goal is to create an operational tool for estimating UV fluxes. In particular, it exploits the recent results on aerosol properties, and TOC produced by the Copernicus Atmosphere Monitoring Service (CAMS) for any location and any time after 2003. The performance of the novel method is assessed by a comparison against high quality measurements of UV fluxes performed in cloud-free conditions. Stations have been selected to fulfill two main constraints as follows: (1) the measurement has to be carried out at cloud-free instant meaning that either it should be clearly marked or using algorithm for selecting cloud-free instants which most of the time needs broadband measurements as inputs, and (2) high quality control and assurance on the measurement. Five stations were such selected which are located at high latitudes.

2. Description of measurements used for comparison

Ground-based measurements were collected from three sites of the UV network of the National Science Foundation (NSF) of the U.S.A. and two sites of the Finnish Meteorological Institute (FMI). Table 1 reports the geographical coordinates of the stations, time period of data and their source, type of instruments, spectral interval and step of measurements.

The site 'Barrow' is located approximately 6 km northeast of the Barrow city in Alaska, on the coast of the Chukchi Sea, part of the Arctic Ocean, usually covered by ice between November

and July. The snow cover of the surroundings of the station extends from October till June. According to Bernhard et al. (2008), the effective UV albedo of the surface reaches its maximum of approximately 0.8 during March-April. It decreases to 0.05 in summer from August until September.

The site 'Sodankylä' is approximately 6 km southwards the village of Sodankylä. The site is located in the vicinity of the river Kitinen, and the surroundings are boreal pine forest and large peatland areas. A permanent snow cover is present during the winter and the annual number of snowy days is on average 190. The snow cover starts accumulating in October or November and melts away during May almost every year. The effective UV albedo follows a seasonal variation due to the snow cover. It ranges from very low values in boreal summer up to 0.65 in winter (Arola et al.; 2003).

Jokioinen Observatory is located in a fairly flat rural area in the southwest of Finland surrounded by fields of agriculture and a boreal forest. The number of snowy days is typically 130. The snow conditions in Jokioinen vary from year to year, and also within each winter. At earliest, snow may appear at the end of October or early November, while it typically melts away in March or April. The effective UV albedo is highly variable; it may rise up to 0.58 in boreal winter but more typical values are 0.2 to 0.5 (Lindfors et al., 2007).

Palmer is situated on the Anvers Island, on the western side of the Antarctic Peninsula. The ocean surrounding the island is frozen during austral winter and usually ice free in summer. According to Bernhard et al. (2005), the effective UV albedo varies between 0.6 and 0.95 occurring from August until November, and then decreases down to 0.3 to 0.5 after snowmelt. It is large even in austral summer because of the glaciers surrounding the site.

McMurdo is a coastal site located on the Ross Island, a volcanic island of Antarctica surrounded by a quasi-persistence of the ice sheet. The surroundings of the station are mostly made of dark volcanic rocks. McMurdo has an annual cycle of change in effective UV albedo. It ranges between 0.54 (March) and 0.99 (October) (Bernhard et al., 2006).

WMO (2008) reports that uncertainties associated with the measurements in UV by spectrometers is difficult to estimate precisely. Beyond the technical specifics of the site itself, several errors may occur in the calibration of the instrument that include *i)* the uncertainties associated with irradiance transfer standards, *ii)* the stability of instruments over time, and *iii)*

imperfect directional response. The WMO guide estimates that a 5% measurement uncertainty at 300 nm can be achieved only under the most rigorous conditions at the present time.

The data provided by the NSF are available online and can be downloaded freely. Only data of version 2, which have been corrected for the instruments' cosine error, have been selected for ensuring higher accuracy. Data measured during clear sky conditions are flagged (flag "CS"). The number of clear sky instants is reported in Table 1. Integrated irradiances in the UV-A and UV-B range are available and have been downloaded from the website http://uv.biospherical.com/Version2.

The data for the two Finnish sites has been corrected for all known errors following the routine spectral UV data processing procedure of the FMI (Lakkala et al., 2008; Mäkelä et al., 2016). The irradiance scale of the FMI's Brewer spectrophotometers is traceable to that maintained by the Finnish National Standards Laboratory at VTT MIKES Metrology and maintained by a rigorous schedule for measurements of primary standard, secondary standard and working standard lamps (Heikkilä et al., 2016a). In this work, the measured UV spectra have been first deconvoluted and then convoluted with a standard triangular slit function with a full width at half maximum (FWHM) of 1 nm and extrapolated using the SHICrivm software package (http://www.rivm.nl/en/Topics/U/UV_ozone_layer_and_climate/SHICrivm) (Slaper et al., 1995, Slaper et al., 1997) to cover the full UV spectrum as explained in Heikkilä et al. (2016b). Spectral irradiances are integrated over the UV-B, and UV-A. The uncertainties related to the extrapolation are less than 2 and 3% to the integrated UV-A, for the Jokioinen and Sodankylä Brewers, respectively, when averaged over daily time window. However, for individual spectra the uncertainties are estimated to be somewhat higher, up to 5-6% for Sodankylä Brewer with the highest measured wavelength at 325nm (Slaper, 2017, personal communication).

In addition, at both Finnish stations, direct, diffuse and global broadband irradiances are measured every 1 min, the global irradiance being the sum of the direct and diffuse irradiances on a horizontal plane. These series of data are exploited for selecting cloud-free instants by using the very restrictive algorithm proposed by Lefèvre et al. (2013). The latter is made of two successive filters. The first one is a constraint on the amount of diffuse irradiance with respect to the global irradiance since the direct irradiance is usually prominent in cloud-free conditions. The second filter analyses the temporal variability of the global irradiance normalized by the irradiance received at the top of the atmosphere and by a typical air mass since this quantity

should be steady for several hours in cloud-free conditions. We assume that a cloud-free instant detected by analyzing broadband irradiances is also cloud-free for the spectral measurements. It is possible that UV is affected by the presence of scattered cloudiness which may go unnoticed in the broadband range and that the retained series of cloud-free instants for broadband may comprise cloudy instants for UV. Given the high selectivity of the algorithm of Lefèvre et al. (2013), we believe that such cases are rare and that the conclusions will be unaffected as a whole.

3. Description of the new method

In brief, the method combines the fluxes estimated by libRadtran in the four KBs and performs a resampling of these fluxes for retrieving UV fluxes. For all the radiative transfer simulations, a plane-parallel atmosphere was assumed and the DISORT 2.0 (discrete ordinate technique) algorithm (Stamnes et al., 2000) with 16 streams was selected to solve the radiative transfer equation because several articles have demonstrated the accuracy of its results when compared to robust and more time consuming solvers.

3.1.   Inputs to libRadtran

In cloud-free conditions, UV irradiance at ground level depends mostly on the SZA θ_s, the ground albedo, the total column content of ozone, the vertical profile of ozone, temperature, pressure, density, and volume mixing ratio for gases as a function of altitude, aerosol optical depth (AOD), Ångström coefficient, aerosol type and the elevation of the ground above sea level. As the method shall be used operationally, the sources of these inputs have been selected to allow estimation of UV irradiance at any location and any time.

The Copernicus Atmosphere Monitoring Service (CAMS) of the European Commission is providing aerosol properties together with physically consistent TOC for any place and any time after 2003. TOC, as well as the AOD at 550 nm, Ångström coefficient, and aerosol type, are collected from this source of data following exactly the path of the McClear model (Lefèvre et al., 2013). θ_s is given by the SG2 algorithm for the sun position and angles (Blanc and Wald, 2012). Ground elevation is extracted from the Shuttle Radar Topography Mission (SRTM)

7

database and has been downloaded from the website
http://srtm.csi.cgiar.org/SELECTION/inputCoord.asp.

The albedo is the ratio of upwelling to downwelling flux at the surface and is the integral of the bidirectional reflectance distribution function (BRDF), which depends on the surface-type, its roughness, and the wavelength of the impinging radiation. A few institutes provide BRDF products in the UV range or Lambert equivalent reflectances (e.g., Herman and Celarier, 1997) covering the world with coarse resolution of 0.5 or 1°. In absence of the ideal solution —BRDF parameters in the UV range available worldwide with a grid cell of 0.05° or better— an approximate solution has been adopted by using the so-called shortwave [250, 5000] nm BRDF parameters proposed by Blanc et al. (2014). The U.S. National Aeronautics and Space Administration (NASA) provides worldwide maps of the BRDF parameters that are derived from the MODIS (Moderate Resolution Imaging Spectroradiometer) instrument (Schaaf et al., 2002). Blanc et al. (2014) have created a series of maps of the MODIS BRDF parameters for each calendar month for the shortwave albedo with no missing values at a spatial resolution of 0.05°. In addition, these authors proposed a method for computing the albedo simultaneously for direct and global irradiances. These maps and this method are those used by the McClear model (Lefèvre et al., 2013). As a first approximation, the UV albedo is assumed to be spectrally constant and equal to the shortwave albedo. This assumption may result in biases depending on the surface. For example, in the case of snow surface, Varotsos et al. (2014) reported from many aircraft measurements that spectral albedo exhibits a tendency to decrease with increasing wavelength, about 0.7 from UV to about 0.4 in the NIR independently of the sky conditions. Therefore, the albedo integrated over the spectrum, becomes less than 0.7 resulting in underestimation in UV albedo, hence in a lesser contribution to diffuse UV irradiance and therefore to underestimation of the global UV.

3.2.   Resampling technique

Let λ be the wavelength, G_λ the global spectral irradiance at the surface and B_λ the direct normal spectral irradiance, i.e. the irradiance received from the direction of the sun at the surface on a plane normal to the sun's rays. The irradiance in a given interval $[\lambda_1, \lambda_2]$ is given by:

$$G_{\lambda1\lambda2} = \int_{\lambda1}^{\lambda2} G_\lambda \, d\lambda \tag{1}$$

Similar expressions may be obtained for irradiances in UV-A, UV-B, UV or over KB$_j$. For example, the UV irradiance G_{UV} and the direct normal irradiance B_{UV} or the irradiance G_{KB4} in KB$_4$ are given by:

$$G_{UV} = \int_{280}^{400} G_\lambda \, d\lambda \tag{2}$$

$$B_{UV} = \int_{280}^{400} B_\lambda \, d\lambda \tag{3}$$

$$G_{KB4} = \int_{307}^{328} G_\lambda \, d\lambda \tag{4}$$

where λ is expressed in nm.

The KBs do not fit exactly the UV spectral ranges. For example, the UV-B is covered by KB$_3$ and a part of KB$_4$. One solution to estimate the irradiance in a UV interval is the use of weighted sums based on the overlap between KB$_j$ and this interval. Another technique is adopted here whose concept is to determine several 1-nm spectral bands NB$_i$ whose transmissivities are correlated to those of the KB$_j$ and then use these transmissivities in a linear interpolation process to compute the UV irradiance. A similar approach has been used by Wandji Nyamsi et al. (2015a) for the calculation of the photosynthetically active radiation with better results than a weighted sum.

If one assumes that the optical properties of the atmosphere do not change over a given NB$_i$, the integrals of Eqs. (2) – (4) may be replaced by Riemann sums over NB$_i$. For example, if λ_i denotes the central wavelength of NB$_i$, G_{UV} can be approximated by:

$$G_{UV} = \sum_{i=1}^{120} G_{\lambda i} \tag{5}$$

If one defines the clearness index KT_i as:

$$KT_i = \frac{G_{\lambda i}}{Eo_i \cos(\theta_s)} \tag{6}$$

where Eo_i is the irradiance at the top of atmosphere on a plane normal to the sun's rays for NB$_i$ for a given instant t, Eq. (5) becomes

$$G_{UV} = \cos(\theta_s) \sum_{i=1}^{120} Eo_i \, KT_i \tag{7}$$

Similarly, the clearness index KT_{KBj} for KB_j is given by:

$$KT_{KBj} = \frac{G_{KBj}}{Eo_{KBj}\cos(\theta_s)} \tag{8}$$

The solar spectrum of Gueymard (2004) available in libRadtran was combined with the algorithm SG2 for computing the sun position (Blanc and Wald, 2012) to yield Eo_i and Eo_{KBj}.

For the method presented here, we assume that simple and accurate relations, e.g. affine functions, may be found between each KT_{KBj} and a sub-set of several KT_i, called KT_k hereafter. Then it may be possible to interpolate linearly between KT_k to obtain an estimate of KT_i for each λ_i. By summing the products of Eo_i and these interpolated KT_i over a given spectral interval, it is then possible to compute the corresponding irradiance. This is the principle of the resampling technique. The set of NB_k is selected at the beginning of the procedure and the same set is used for all processing. The number of NB_k should be as small as possible in order to decrease the amount of calculations but still large enough to allow a good accuracy.

The selection of NB_k is empirically determined by means of libRadtran. The current approach is empirical with no guarantee that the selected set of NB_k is the optimum. It could have been possible to use some mathematical optimisation tools. This is not a straightforward process as the cost function should take into account that the number of NB_k is unknown *a priori*.

A set of 60 000 clear sky atmospheric states was built by means of the Monte-Carlo technique in order to select NB_k. Each state comprises the nine variables described above, and the value of each variable was randomly selected by taking into account their modelled marginal distribution. The distributions proposed by Lefèvre et al. (2013) and Oumbe et al. (2011) established from observations were adopted here (Table 2). More specially, the uniform distribution is chosen as a model for marginal probability for all variables except AOD, Angstrom exponent coefficient, and total column content of ozone. The chi-square law for AOD, the normal law for the Angstrom exponent coefficient, and the beta law for TOC have been selected. The selection of these parametric probability density functions and their corresponding parameters have been empirically determined from the analyses of the observations made in the AERONET network for aerosol properties and from meteorological satellite-based ozone products (Lefèvre et al., 2013).

Each atmospheric state is input twice to libRadtran, (1) with the Kato et al. approach yielding KT_{KB3}, KT_{KB4}, KT_{KB5} and KT_{KB6}, and (2) with detailed spectral computations providing KT_i every 1 nm for the interval [283, 408] nm. Several plots were made superimposing KT_{KB3}, KT_{KB4}, KT_{KB5} and KT_{KB6} (in green) and KT_i (in red). Figure 1 is such a graph with the following inputs: Θ_s of 53.76°, *midlatitude winter* atmospheric profile, TOC of 470 DU, AOD of 0.78 at 1000 nm for a maritime polluted aerosol model with an Ångstrom exponent of 1.93, elevation of 0 m and surface albedo of 0.63. A visual inspection shows that KT_{KBj} and KT_i are approximately equal for λ_j in the middle of KB_j, except for KB_5. KT_i in this band exhibits a non-linear behaviour that cannot be accounted for with a single KT_k. If one selects 305, 320, 333, 346 and 386 nm as NB_k (magenta crosses), then the linear interpolation (in blue) provides a fairly accurate estimate of KT_i. The five NB_k were selected by a lengthy visual inspection of such plots and are reported in Table 3. The same NB_k apply for the global and direct irradiances. For each NB_k, the parameters of the affine function relating KT_{KBj} and KT_k are determined by least-square fitting technique (Table 3):

$$KT_k = a_k\, KT_{KBj} +\, b_k \tag{9}$$

Another set of parameters is determined in the same way for the direct irradiance. In the operational mode, given an atmospheric state, a run of libRadtran, or a fast approximation of it, yields four KT_{KBj}, from which the five KT_k are computed using the affine functions. Then, approximate KT_i* are computed for each nm between 280 and 400 nm using a linear interpolation and extrapolation of KT_k. In case extrapolation provides negative values, KT_i* is set to 0. Eventually, G_{UV} is obtained by

$$G_{UV} = cos(\Theta_s)\, \sum_{i=1}^{120} Eo_i\ KT_i^* \tag{10}$$

A similar process is performed for the direct normal irradiance B_{UV} as well as for the same quantities in UV-A and UV-B. As the method provides the spectrum KT_i*, the equation may be extended to include any action spectrum $S(\lambda)$, e.g.:

$$G_{S(\lambda)} = cos(\Theta_s)\, \sum_{\lambda1}^{\lambda2} Eo_i\, S(i)\, KT_i^* \tag{11}$$

3.3.   Numerical validation

In this section, results of the proposed technique are compared with results from the detailed spectral calculations made by libRadtran to assess the accuracy of the proposed technique for G_{UVA}, G_{UVB}, B_{UVA} and B_{UVB} for cloud-free conditions. The errors made by using the proposed technique for calculations of the UV-A and UV-B irradiances are presented. To that extent, an additional sample of 10 000 atmospheric states has been randomly constructed following the marginal distribution variables described in Table 2. The proposed technique was applied to the outputs of libRadtran using Kato et al. approach and the estimates were compared to the detailed calculations performed by libRadtran. Following the ISO standard (1995), the deviations were computed by subtracting measurements for each instant from the results of the method. They were summarized by the bias (mean error), the root mean square error (RMSE), and their values *rbias* and *rRMSE* relative to the mean value of the measurements. In addition, the coefficient of determination (R^2) is computed.

Table 4 reports the statistical indicators for the global and direct normal UV-A, UV-B irradiances. For UV–A fluxes, the bias for the global irradiance and the direct irradiance, is +0.10 W m^{-2}, i.e. +0.2% in relative value, and -0.15 W m^{-2}, i.e. -0.7% in relative value, respectively. The RMSE is respectively 0.12 W m^{-2} (0.3%) and 0.18 W m^{-2} (0. 8%). For UV–B fluxes, the bias for the global irradiance and the direct irradiance, is -0.04 W m^{-2}, i.e. -1.6% in relative value, and +0.07 W m^{-2}, i.e. +10.1% in relative value, respectively. The corresponding RMSE is respectively 0.14 W m^{-2} (6.2%) and 0.15 W m^{-2} (20.5%). The coefficient of determination R^2 is greater than 0.99 except for the direct normal UV-B irradiance which is 0.966. Expectedly, these indicators prove the good level of performance of the proposed technique.

4. Results

The results of the proposed method were compared to measurements of UV–A and UV–B irradiances at the surface for cloud-free conditions. Similar statistical indicators as those presented in the previous section are also computed to synthetize the errors.

4.1.   Performance of the method for UV–A irradiance

12

Figure 2 exhibits the scatter density plot between ground-based instantaneous measurements made for each station in cloud-free conditions and estimates from the proposed method combined with inputs from CAMS. The station name is indicated at top of the plot of each plot. Figure 2a exhibits the results for Barrow. All points are well located along the identity line. The slope of the fitting line is 0.995, i.e. very close to 1, showing a very good estimation of the measurements by the method. R^2 is 0.97, meaning that all the variability in the measurements is very well explained by the estimates. The bias is low: -0.2 W m^{-2}, i.e. -1% of the mean value of the measurements: 20.5 W m^{-2}. The RMSE is small: 1.4 W m^{-2}, around 7% of the mean. These statistical indicators for each station are reported in Table 5. The measurements are mostly between March and September. The shortwave albedo is 0.8 from the beginning of March till the middle of May. With the progressive snowmelt, this shortwave albedo decreases from mid-May down to 0.12 at mid-July. This variation corresponds well to the climatological evolution reported by Bernhard et al. (2008) and supports the choice of this approximation by the shortwave albedo.

Even if the points follows quite well the perfect line (Figure 2a), a set of points is seen where the method underestimate noticeably by more than 20%. These underestimations occurs between ending May and mid-July. During that period, the shortwave albedo was less than the effective UV albedo by a factor 0.8. The effective UV albedo is part of the Version 2 dataset and was derived by comparing measured clear-sky spectra with corresponding radiative transfer model results (Bernhard et al., 2007). As a smaller albedo means a smaller contribution to the diffuse part of the irradiance, the difference between the shortwave and effective UV albedo may explain these underestimations seen in Figure 2a.

Results for Sodankylä are shown in Figure 2b. Cloud-free conditions occur mostly between February and September. The points lie along the identity line with a slight overestimation by the method at low irradiance and an underestimation at large irradiance. R^2 is 0.98. The bias is low: -0.5 W m^{-2}, i.e. -2% of the mean value: 20.8 W m^{-2}. The RMSE is low: 1.9 W m^{-2} (9%). As for Jokioinen (Figure 2c), all points are well located along the identity line. R^2 is 0.98. The bias is low: -0.5 W m^{-2}, i.e. -2% of the mean value of the measurements: 22.1 W m^{-2}, as well as the RMSE: 1.6 W m^{-2} (8%).

Results for Palmer are shown in Figure 2d. One may note that the points are well aligned with low scatter along a straight line whose slope is 0.99 with a slight underestimation by the

method. The bias is -0.8 W m^{-2} (-3% of the mean value of 24.9 W m^{-2}). The RMSE is 1.2 W m^{-2} (5%). R^2 is greater than 0.99. Cloud-free conditions occur mostly between August and April. The shortwave albedo slightly increases from 0.28 to 0.32 between August and March, then decreases until April up to 0.20. These values are small and close to those of a ground free of snow or ice. The effective UV albedo is usually greater than 0.3 with peaks up to 0.8. This difference between the shortwave and effective UV albedo may explain the slight underestimation indicated in Figure 5.

Results for McMurdo are shown in Figure 2e. Cloud-free conditions occur mostly between April and September. The points are aligned along the identity line. R^2 is 0.99. The bias is low: -0.3 Wm^{-2} (-1% of the mean value: 21.0 W m^{-2}), as well as the RMSE: 1.2 W m^{-2} (6%). The shortwave albedo may reach 0.8 and there is no clear discrepancy between the shortwave and effective UV albedo. Nevertheless, the authors believe that the outliers may be explained by a difference in albedo.

The dependence of errors by SZA was investigated. Figure 3 exhibits the ratio (top) and difference (bottom) as function of Θ_s for each station for UV-A irradiances. For the ratio, the limits of boxes are close from one quartile to another meaning a very limited spread of the ratio. The deviations between maximum and minimum are approximately small. The median is similar to the mean. Whatever the number of data (in pink color), they are very close to 1 for all SZA ranges and stations except Sodankylä at high Θ_s. As for the ratio, the similar observations are also seen in terms of the differences at bottom of Figure 3. The difference is very close to 0 for all the SZA ranges. The absolute value of the mean difference shows a tendency to decrease as Θ_s increases, with the maximum reached for low Θ_s.

The dependence of errors by TOC and albedo was also investigated (not shown). The results have revealed that there is no clear dependence of errors by TOC or albedo for all stations. In addition, the absolute values of the bias (not shown) show a tendency to decrease as Θ_s increases, with the maximum reached for low Θ_s, except McMurdo. In the opposite manner, the absolute values of the relative bias show a tendency to increase with Θ_s. This could be related to the fact that low Θ_s are reached in summer with greater values in UV irradiance and lower values in effective UV albedo.

4.2.   Performance of the method for UV-B irradiance

14

The UV-B band is the spectral region of UV irradiance where the ozone absorption is very strong. Figure 4 exhibits the scatter density plots between measurements of UV-B and estimates for each station. Table 6 reports the statistical indicators for UV-B. R^2 is greater than 0.97 for all stations, meaning that variability in UV-B is very well reproduced by the estimates. In general, the method overestimates the UV-B irradiances. Visually, one observes that the method clearly overestimates when the irradiance is low. For the wavelength less than 320 nm, in Figure 1, the proposed method seems to mostly overestimate when compared to the detailed spectral calculations serving as reference. This observation induces a systematic overestimation at low irradiance from the method. This mainly explains this previous observation. The absolute value of the bias is less than 0.1 W m^{-2}. The relative bias ranges between –4% (Palmer) and 13% (Barrow). rRMSE ranges between 12% and 18%.

Figure 5 shows the change in ratio and relative difference as a function of Θ_s. For both ratio and differences, the spread of limits of boxes is more or less visible. Nevertheless, the median and the mean are close. It shows a tendency to increase with Θ_s for all stations meaning probably a systematic bias from the method more visible at high Θ_s as mentioned above. This results explained the main sources of errors for the dependence of errors by TOC and albedo.

In addition, (not shown), one notices a tendency of the bias to reach a maximum between 65° and 75°; this appears in the form of a plateau around 65° for the RMSE which decreases as Θ_s increases, i.e. as the irradiance decreases. The relative bias increases with Θ_s as well as the rRMSE. Both are closer in the high Θ_s than in the small Θ_s.

5. Discussion and Conclusion

The comparison has demonstrated a reasonable agreement between the ground-based measurements of UV-A and UV-B and the estimates by the proposed method with CAMS products as inputs. The variability in UV fluxes is well reproduced by the method. A good level of accuracy is reached that is close to the uncertainty of the measurements themselves. The computations of the fluxes in the KBs can be performed quite fast with the use of pre-computed abaci as shown by the example of the McClear model. This model is an accurate approximation of libRadtran but 10^5 times faster. The proposed method extends the results of the McClear model to the UV range and can be used in future operational tools that are both accurate and fast.

Further improvements are needed. A major improvement would be the extension to all sky conditions. In this aspect, one may build on the work of Oumbe et al. (2014) who demonstrated that, in the case of an infinite plane-parallel single- and double-layered cloud, the solar irradiance at ground level computed by a radiative transfer model can be approximated by the product of the irradiance under clear atmosphere and a modification factor that depends on cloud properties and ground albedo only as changes in clear-atmosphere properties have negligible effect on this factor. Such an approximation has been exploited previously with limited justification by several authors in studies on broadband irradiance (Huang et al., 2011), UV or photosynthetically active radiation (see e.g. Calbo et al., 2005; den Outer et al., 2010; Krotkov et al., 2001).

Another improvement consists in the modelling of the surface albedo in the UV range. Maps of BRDF parameters in the UV range must be created with a satisfactory spatial resolution of 0.05° or better. The MODIS BRDF parameters may be a starting point as they are available at several wavelengths. It could be possible to apply the technique used by Blanc et al. (2014) to create BRDF maps for each wavelength and for each calendar month with no missing values. The smallest wavelength in the MODIS BRDF is approximately 470 nm, i.e. outside the UV range, and extrapolation towards small wavelengths will be necessary.

6. Data availability

UV data from Barrow, Palmer Station and McMurdo Station were provided by the NSF UV Monitoring Network, operated by Biospherical Instruments Inc. and funded by the U.S. National Science Foundation's Office of Polar Programs. Version 2 data used here are available from http://uv.biospherical.com/Version2/Version2.asp

FMI's spectral Brewer UV measurements are available through the European UV Data Base: http://uv.fmi.fi/uvdb/

Products from CAMS can be downloaded from the web site: http://atmosphere.copernicus.eu/

The BRDF maps by Blanc et al. (2014) may be downloaded from the web site: http://www.oie.mines-paristech.fr/Valorisation/Outils/AlbedoSol/

5 **References**

Aculinin, A., Brogniez, C., Bengulescu, M., Gillotay, D., Auriol, F., and Wald, L.: Assessment of several empirical relationships for deriving daily means of UV–A irradiance from Meteosat–based estimates of the total irradiance, *Remote Sensing*, 8, 537, doi:10.3390/rs8070537, 2016.

Arola, A., Kaurola, J., Koskinen, L., Tanskanen, A., Tikkanen, T., Taalas, P., and Fioletov, V.:
10 A new approach to estimating the albedo for snow-covered surfaces in the satellite UV method, *J. Geophys. Res.-Atmos.*, 1984–2012, 108(D17), 2003.

Bernhard, G., Booth, C. R., and Ehramjian, J. C.: UV climatology at Palmer Station, Antarctica, based on version 2 NSF network data, In Proc. of SPIE Vol. 5886, 588607-01, doi: 10.1117/12.614172, 2005.

15 Bernhard, G., Booth, C.R., Ehramjian, J.C., Stone, R. and Dutton, E.G.: Ultraviolet and visible radiation at Barrow, Alaska: Climatology and influencing factors on the basis of version 2 National Science Foundation network data. *J. Geophys. Res: Atmospheres*, 112(D9), 2007.

Bernhard, G., Booth, C. R. and Ehramjian, J. C.: Comparison of UV irradiance measurements at Summit, Greenland; Barrow, Alaska; and South Pole, Antarctica, *Atmos. Chem. Phys.*, 8,
20 4799-4810, 2008.

Blanc, P., Gschwind, B., Lefèvre, M., and Wald, L.: The HelioClim project: Surface solar irradiance data for climate applications, *Remote Sensing*, 3, 343-361, doi:10.3390/rs3020343, 2011.

Blanc, P., Gschwind, B., Lefèvre, M., and Wald, L.: Twelve monthly maps of ground albedo
25 parameters derived from MODIS data sets. In Proceedings of IGARSS 2014, held 13-18 July 2014, Quebec, Canada, USBKey, pp. 3270-3272, 2014. Data available at http://www.oie.mines-paristech.fr/Valorisation/Outils/AlbedoSol/

Blanc, P., and Wald, L.: The SG2 algorithm for a fast and accurate computation of the position of the Sun, *Sol. Energy*, 86, 3072-3083, doi: 10.1016/j.solener.2012.07.018, 2012.

30 Calbó, J., Pages, D., and González, J. A.: Empirical studies of cloud effects on UV radiation: A review, *Rev. Geophys.*, 43(2), 2005.

17

Canada, J., Pedros, G., Lopez, A., and Bosca, J.V.: Influences of the clearness index for the whole spectrum and of the relative optical air mass on UV solar irradiance for two locations in the Mediterranean area, Valencia and Cordoba, *J. Geophys. Res.*, 105, 4759–4766, 2003.

Coste, A., Goujon, S., Boniol, M., Marquant, F., Faure, L., Doré, J.-F., Hémon, D., and Clavel, J.: Residential exposure to solar ultraviolet radiation and incidence of childhood hematological malignancies in France, *Cancer Causes Control*, 26, 1339–1349, 2015.

de Gruijl, F. R., Sterenborg, H. J., Forbes, P. D., Davies, R. E., Cole, C., Kelfkens, G., van Weelden, H., Slaper, H. and van der Leun, J. C.: Wavelength dependence of skin cancer induction by ultraviolet irradiation of albino hairless mice, *Cancer research*, 53(1), 53-60, 1993.

Delcourt, C., Cougnard-Grégoire, A., Boniol, M., Carrière, I., Doré, J.-F., Delyfer, M.-N. Rougier, M.-B., Le Goff, M., Dartigues, J.-F., Barberger-Gateau, P., and Korobelnik, J.F.: Lifetime exposure to ambient ultraviolet radiation and the risk for cataract extraction and age-related macular degeneration: The Alienor study, *Investig. Ophthalmol. Vis. Sci.*, 55, 7619–7627, 2014.

den Outer, P. N., Slaper, H., Kaurola, J., Lindfors, A., Kazantzidis, A., Bais, A. F., Feister, U., Junk, J., Janouch, M., and Josefsson, W.: Reconstructing of erythemal ultraviolet radiation levels in Europe for the past 4 decades, *J. Geophys. Res. Atmos.*, 115, D10102, doi:10.1029/2009JD012827, 2010.

Emde, C., Buras-Schnell, R., Kylling, A., Mayer, B., Gasteiger, J., Hamann, U., Kylling, J., Richter, B., Pause, C., Dowling, T., and Bugliaro, L.: The libRadtran software package for radiative transfer calculations (version 2.0.1), *Geosci. Model Dev.*, 9, 1647-1672, doi:10.5194/gmd-9-1647-2016, 2016.

Fortes, C., Mastroeni, S., Bonamigo, R., Mannooranparampil, T., Marino, C., Michelozzi, P., Passarelli, F., and Boniol, M.: Can ultraviolet radiation act as a survival enhancer for cutaneous melanoma? *Eur. J. Cancer Prev.*, 25, 34–40, 2016.

Foyo-Moreno, I., Vida, J., and Alados-Arboledas, L.: Ground-based ultraviolet (290–385 nm) and broadband solar radiation measurements in South-eastern Spain, *Int. J. Climatol.*, 18, 1389–1400, 1998.

Gueymard, C.: The sun's total and the spectral irradiance for solar energy applications and solar radiations models, *Sol. Energy*, 76, 423-452, 2004.

Heikkilä, A., Sakari Mäkelä, J., Lakkala, K., Meinander, O., Kaurola, J., Koskela, T., Karhu, J. M., Karppinen, T., Kyrö, E., and de Leeuw, G.: In search of traceability: two decades of

calibrated Brewer UV measurements in Sodankylä and Jokioinen, *Geosci. Instrum. Method. Data Syst.*, 5, 531-540, doi: 10.5194/gi-5-531-2016, 2016a

Heikkilä, A., Kaurola, J., Lakkala, K., Karhu, J. M., Kyrö, E., Koskela, T., Engelsen, O., Slaper, H., and Seckmeyer, G.: European UV DataBase (EUVDB) as a repository and quality analyser for solar spectral UV irradiance monitored in Sodankylä, *Geosci. Instrum. Method. Data Syst.*, 5, 333-345, doi: 10.5194/gi-5-333-2016, 2016b

Herman, J. R. and Celarier, E. A.: Earth surface reflectivity climatology at 340 nm to 380 nm from TOMS data, *J. Geophys. Res.*, 102, 28 003–28 011, 1997.

Huang, G. H., Ma, M. G., Liang, S. L., Liu, S. M., and Li, X.: A LUT-based approach to estimate surface solar irradiance by combining MODIS and MTSAT data, *J. Geophys. Res.-Atmos.*, 116, D22201, doi:10.1029/2011JD016120, 2011.

ISO Guide to the Expression of Uncertainty in Measurement: first edition, International Organization for Standardization, Geneva, Switzerland, 1995.

Juzeniene, A., Brekke, P., Dahlback, A., Andersson–Engels, S., Reichrath, J., Moan, K., Holick, M.F., Grant, W.B., and Moan, J.: Solar radiation and human health, *Rep. Prog. Phys.* 74(6), 066701, doi:10.1088/0034–4885/74/6/066701, 2011.

Kato, S., Ackerman, T., Mather, J., and Clothiaux, E.: The *k*-distribution method and correlated-*k* approximation for shortwave radiative transfer model, *J. Quant. Spectrosc. Radiat. Transf.*, 62, 109-121, 1999.

Kravietz, A., Ka, S., Wald, L., Dugravot, A., Singh-Manoux, A., Moisan, F., Elbaz, A.: Association of UV radiation with Parkinson disease incidence: a nationwide French ecologic study, *Env Res*, 154, 50-56, doi: 10.1016/j.envres.2016.12.008, 2017.

Krotkov, N. A., Herman, J. R., Bhartia, P. K., Fioletov, V., and Ahmad, Z.: Satellite estimation of spectral surface UV irradiance: 2. Effects of homogeneous clouds and snow, *J. Geophys. Res.-Atmos.*, 106(D11), 11743-11759, 2001.

Lakkala, K., Arola, A., Heikkilä, A., Kaurola, J., Koskela, T., Kyrö, E., Lindfors, A., Meinander, O., Tanskanen, A., Gröbner, J., and Hülsen, G.: Quality assurance of the Brewer spectral UV measurements in Finland, *Atmos. Chem. Phys.*, 8, 3369–3383, doi:10.5194/acp-8-3369-2008, 2008.

Lefèvre, M., Blanc, P., Espinar, B., Gschwind, B., Ménard, L., Ranchin, T., Wald, L., Saboret, L., Thomas, C., and Wey, E.: The HelioClim-1 database of daily solar radiation at Earth surface: an example of the benefits of GEOSS Data-CORE, *IEEE J-STARS*, 7, 1745-1753, doi:10.1109/JSTARS.2013.2283791, 2014.

Lefèvre, M., Oumbe, A., Blanc, P., Espinar, B., Gschwind, B., Qu, Z., Wald, L., M. Schroedter-Homscheidt, Hoyer-Klick, C., Arola, A., Benedetti, A., Kaiser, J.W., and Morcrette, J.-J.: McClear: a new model estimating downwelling solar radiation at ground level in clear-sky conditions, *Atmos. Meas. Tech.*, 6, 2403-2418, 2013.

5 Lindfors, A., Heikkilä, A., Kaurola, J., Koskela, T., and Lakkala, K.: Reconstruction of solar spectral surface UV irradiances using radiative transfer simulations, *Photochem. Photobiol.*, 85, 1233–1239, 2009.

Lindfors, A., Kaurola, J., Arola, A., Koskela, T., Lakkala, K., Josefsson, W., Olseth, J. A., and Johnsen, B.: A method for reconstruction of past UV radiation based on radiative transfer

10 modeling: Applied to four stations in northern Europe, *J. Geophys. Res.*, 112, D23201, doi:10.1029/2007JD008454, 2007.

Mäkelä, J. S., Lakkala, K., Koskela, T., Karppinen, T., Karhu, J. M., Savastiouk, V., Suokanerva, H., Kaurola, J., Arola, A., Lindfors, A. V., Meinander, O., de Leeuw, G., and Heikkilä, A.: Data flow of spectral UV measurements at Sodankylä and Jokioinen, *Geosci.*

15 *Instrum. Method. Data Syst.*, 5, 193-203, doi:10.5194/gi-5-193-2016, 2016.

Mayer, B., and Kylling, A.: Technical note: The libRadtran software package for radiative transfer calculations-description and examples of use, *Atmos. Chem. Phys.*, 5, 1855-1877, 2005.

Mayer, B., Seckmeyer, G., and Kylling, A.: Systematic long-term comparison of spectral UV

20 measurements and UVSPEC modeling results, *J. Geophys. Res.-Atmos.*, 102(D7), 8755–8768, 1997.

McKinlay, A. F. and Diffey, B. L.: A reference action spectrum for ultraviolet induced erythema in human skin, The CIE Journal, 6, 17–22, 1987.

Mesrine, S., Kvaskoff, M., Bah, T., Wald, L., Clavel–Chapelon, F., and Boutron–Ruault, M.–

25 C.: Nevi, ambient ultraviolet radiation and thyroid cancer risk: a French prospective study. *Epidemiology*, in press, doi: 10.1097/EDE.0000000000000673, 2017.

Norval, M.: The effect of ultraviolet radiation on human viral infections, *Photochem. Photobiol.*, 82, 1495–504, 2006.

Norval, M., and Halliday, G.M.: The consequences of UV-induced immunosuppression for

30 human health, *Photochem. Photobiol.*, 87, 965–977, doi:10.1111/j.1751-1097.2011.00969.x, 2011.

Orton, S.–M., Wald, L., Confavreux, C., Vukusic, S., Krohn, J.P., Ramagopalan, S.V., Herrera, B.M., Sadovnick, A.D., and Ebers, G.C.: Association of UV radiation with multiple sclerosis

prevalence and sex ratio in France, *Neurology*, 76, 425–431, doi: 10.1212/WNL.0b013e31820a0a9f, 2011.

Oumbe, A., Blanc, P., Gschwind, B., Lefevre, M., Qu, Z., Schroedter-Homscheidt, M., and Wald, L.: Solar irradiance in clear atmosphere: study of parameterisations of change with

5   altitude, *Adv. Sci. Res.*, 6, 199-203, 2011.

Oumbe, A., Qu, Z., Blanc, P., Lefèvre, M., Wald, L., and Cros, S.: Decoupling the effects of clear atmosphere and clouds to simplify calculations of the broadband solar irradiance at ground level, *Geosci. Model Dev.*, 7, 1661-1669, doi:10.5194/gmd-7-1661-2014, 2014. Corrigendum, 7, 2409-2409, 2014.

10   Schaaf, C.B., Gao, F., Strahler, A.H., Lucht, W., Li, X.W., Tsang, T., Strugnell, N.C., Zhang, X.Y., Jin, Y.F., Muller, J.P., Lewis, P., Barnsley, M., Hobson, P., Disney, M., Roberts, G., Dunderdale, M., Doll, C., d'Entremont, R.P., Hu, B.X., Liang, S.L., Privette, J.L., and Roy, D.: First operational BRDF, albedo nadir reflectance products from MODIS, *Remote Sens. Environ.*, 83, 135-148, doi:10.1016/S0034-4257(02)00091-3, 2002.

15   Slaper, H. and Koskela, T.: Methodology of intercomparing spectral sky measurements, correcting for wavelength shifts, slit function differences and defining a spectral reference, in: The Nordic intercomparison of ultraviolet and total ozone instruments at Izana, October 1996. Izana: *Meteorological Publications 36*, edited by: Kjeldstad, B., Johnson, B., and Koskela, T., Finnish Meteorological Institute, 89 pages, 1997.

20   Slaper, H., Reinen, H., Blumthaler, M., Huber, M., and Kuik, F.: Comparing ground-level spectrally resolved solar UV measurements using various instruments: A technique resolving effects of wavelength shift and slit width, *Geophys. Res. Lett*., 22, 2721-2724, 1995.

Setlow, R. B., Grist, E., Thompson, K. and Woodhead, A.D.: Wavelengths effective in induction of malignant melanoma, *Proceedings of the National Academy of Sciences*, 90(14),

25   6666-6670, 1993.

Stamnes, K., Tsay, S.-C., Wiscombe, W., and Laszlo, I.: DISORT, a general purpose Fortran program for discrete ordinate method radiative transfer in scattering and emitting layered media: Documentation of methodology. - Tech. Rep., Dept. of Physics and Engineering Physics, Stevens Institute of Technology, Hoboken, NJ07030, USA, 2000.

30   Tanskanen, A., Lindfors, A., Maatta, A., Krotkov, N., Herman, J., Kaurola, J., Koskela, T., Lakkala, K., Fioletov, V., Bernhard, G., McKenzie, R., Kondo, Y., O'Neill, M., Slaper, H., den Outer, P., Bais, A. F., and Tamminen, J.: Validation of daily erythemal doses from Ozone

Monitoring Instrument with ground-based UV measurement data, *J. Geophys. Res.-Atmos.*, 112, D24S44, doi: 10.1029/2007JD008830, 2007.

Varotsos, C. A., Melnikova, I. N., Cracknell, A. P., Tzanis, C., and Vasilyev, A. V.: New spectral functions of the near-ground albedo derived from aircraft diffraction spectrometer observations, *Atmos. Chem. Phys.*, 14, 6953–6965, doi:10.5194/acp-14-6953-2014, 2014.

Wandji Nyamsi, W., Espinar, B., Blanc, P., and Wald, L.: How close to detailed spectral calculations is the *k*-distribution method and correlated-*k* approximation of Kato et al. (1999) in each spectral interval?, *Meteorol. Z.*, 23, 547-556, doi: 10.1127/metz/2014/0607, 2014.

Wandji Nyamsi, W., Espinar, B., Blanc, P., and Wald, L.: Estimating the Photosynthetically Active Radiation in clear sky conditions from the k-distribution method and correlated-k approximation of Kato et al. (1999), *Adv. Sci. Res.*, 12, 5-10, doi:10.5194/asr-12-5-2015, 2015a.

Wandji Nyamsi, W., Arola, A., Blanc, P., Lindfors, A. V., Cesnulyte, V., Pitkänen, M. R. A., and Wald, L.: Technical Note: A novel parameterization of the transmissivity due to ozone absorption in the *k*-distribution method and correlated-*k* approximation of Kato et al. (1999) over the UV band, *Atmos. Chem. Phys.*, 15, 7449-7456, doi: 10.5194/acp-15-7449-2015, 2015b.

WMO *Guide to Meteorological Instruments and Methods of Observation*, WMO-No. 8 (2008 edition, Updated in 2010), World Meteorological Organization, Geneva, Switzerland, 2008.

Table 1: Description of stations used for validation, ordered by decreasing latitude

Station	Barrow	Sodankylä	Jokionen	Palmer	McMurdo
Source	NSF	FMI	FMI	NSF	NSF
Latitude (°)	71.32	67.37	60.82	-64.77	-77.83
Longitude (°)	-156.68	26.63	23.50	-64.05	166.67
Altitude (m)	8	179	104	21	183
Instrument	SUV-100 spectro radiometer	Brewer spectro radiometer MK-II#037	Brewer spectro radiometer MK-III #107	SUV-100 spectro radiometer	SUV-100 spectro radiometer
Average acquisition frequency	4 spectra per hour	Between 1 and 2 spectra per hour	Between 1 and 2 spectra per hour	4 spectra per hour	4 spectra per hour
Spectral range (nm)	280-600	290-325	286.5-365	280-600	280-600
Step (nm)	0.2 in UV-B to 1.0 in visible	0.5	0.5	0.2 in UV-B to 1.0 in visible	0.2 in UV-B to 1.0 in visible
Period	2005-01 to 2010-11	2007-01 to 2011-12	2007-01 to 2008-12	2005-01 to 2010-09	2005-01 to 2010-02
NCFI*	4293	2590	1140	1736	10175

*NCFI: Number of cloud-free instants.

Table 2. Ranges and statistical distributions of values taken by the cosine of the solar zenith angle, the ground albedo and the 7 variables describing the clear atmosphere

Variable	Value
Cosine of the SZA cos Θs	Uniform between 0 and 89 (degree) for Θs
Ground albedo ρg	Uniform between 0 and 0.9
Elevation of the ground above mean sea level	Equiprobable in the set: {0, 1, 2, 3} (km)
Total column content of ozone	Ozone content is: $300*\beta + 200$, in Dobson unit. Beta distribution, with A parameter = 2, and B parameter = 2, to compute β
Atmospheric profiles (Air Force Geophysics Laboratory standards)	Equiprobable in the set {"Midlatitude Summer", "Midlatitude Winter", "Subarctic Summer", "Subarctic Winter", "Tropical", "US. Standard"}
Aerosol optical depth at 550 nm	Gamma distribution, with shape parameter = 2, and scale parameter = 0.13
Angstrom exponent coefficient	Normal distribution, with mean=1.3 and standard-deviation=0.5
Aerosol type	Equiprobable in the set {"urban", "rural", "maritime", "tropospheric", "desert", "continental", "Antarctic"}

Table 3. KB covering UV band and selected sub-intervals NB_k, slopes and intercepts of the affine functions between the clearness indices in KB and sub-intervals NB_k.

KB	KB range, nm	Sub-interval NB_k, nm (# k)	Global		Direct normal	
			Slope a_i	Intercept b_i	Slope c_i	Intercept d_i
3	283 – 307	304 – 305 (#1)	3.0900	0.0007	3.0852	0.0003
4	307 – 328	319 – 320 (#2)	1.1264	-0.0175	1.0886	-0.0007
5	328 – 363	332 – 333 (#3)	1.0247	-0.0519	0.8992	-0.0103
		345 – 346 (#4)	0.9946	0.0152	1.0112	-0.0004
6	363 – 408	385 – 386 (#5)	1.0030	-0.0032	0.9987	-0.0023

5

Table 4. Statistical indicators of the performances of the proposed technique for estimating UV fluxes

UV fluxes	Mean (W m^{-2})	Bias (W m^{-2})	RMSE (W m^{-2})	rBias (%)	rRMSE (%)	R^2
G_{UVA}	45.6	+0.1	0.1	+0.2	0.2	1.00
B_{UVA}	23.4	-0.1	0.2	-0.6	0.8	1.00
G_{UVB}	2.30	-0.04	0.14	-1.64	6.19	1.00
B_{UVB}	0.73	+0.07	0.15	+10.10	20.48	0.97

5

Table 5. Statistical indicators of the performances of the method for UV-A irradiance. N is the number of data points.

Station	N	Mean (W m^{-2})	Bias (W m^{-2})	RMSE (W m^{-2})	rBias (%)	rRMSE (%)	R^2
Barrow	4293	20.0	-0.2	1.4	-1.1	6.8	0.98
Sodankylä	2590	20.8	-0.5	1.9	-2.5	9.0	0.98
Jokioinen	1140	22.1	-0.5	1.6	-2.1	7.5	0.98
Palmer	1736	24.9	-0.8	1.2	-3.1	4.9	0.99
McMurdo	10175	20.3	-0.3	1.1	-1.6	5.6	0.99

5

Table 6. Statistical indicators of the performances of the method for UV-B irradiance. N is the number of data points.

Station	N	Mean (W m^{-2})	Bias (W m^{-2})	RMSE (W m^{-2})	rBias (%)	rRMSE (%)	R^2
Barrow	4293	0.57	0.08	0.10	13.41	18.01	0.97
Sodankylä	2590	0.65	0.05	0.09	7.74	13.91	0.98
Jokioinen	1140	0.75	0.05	0.10	6.70	13.74	0.98
Palmer	1736	1.03	−0.04	0.12	−4.24	11.67	0.99
McMurdo	10175	0.72	0.04	0.09	4.86	12.32	0.98
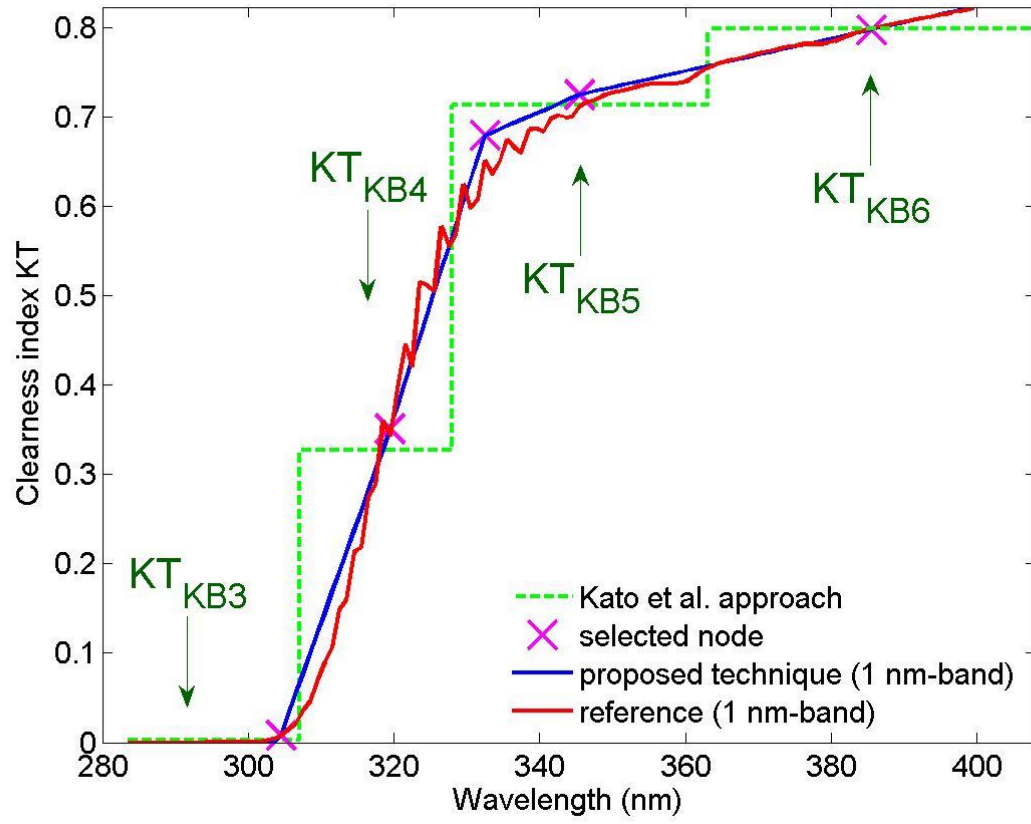
Figure 1: Illustration of the resampling technique
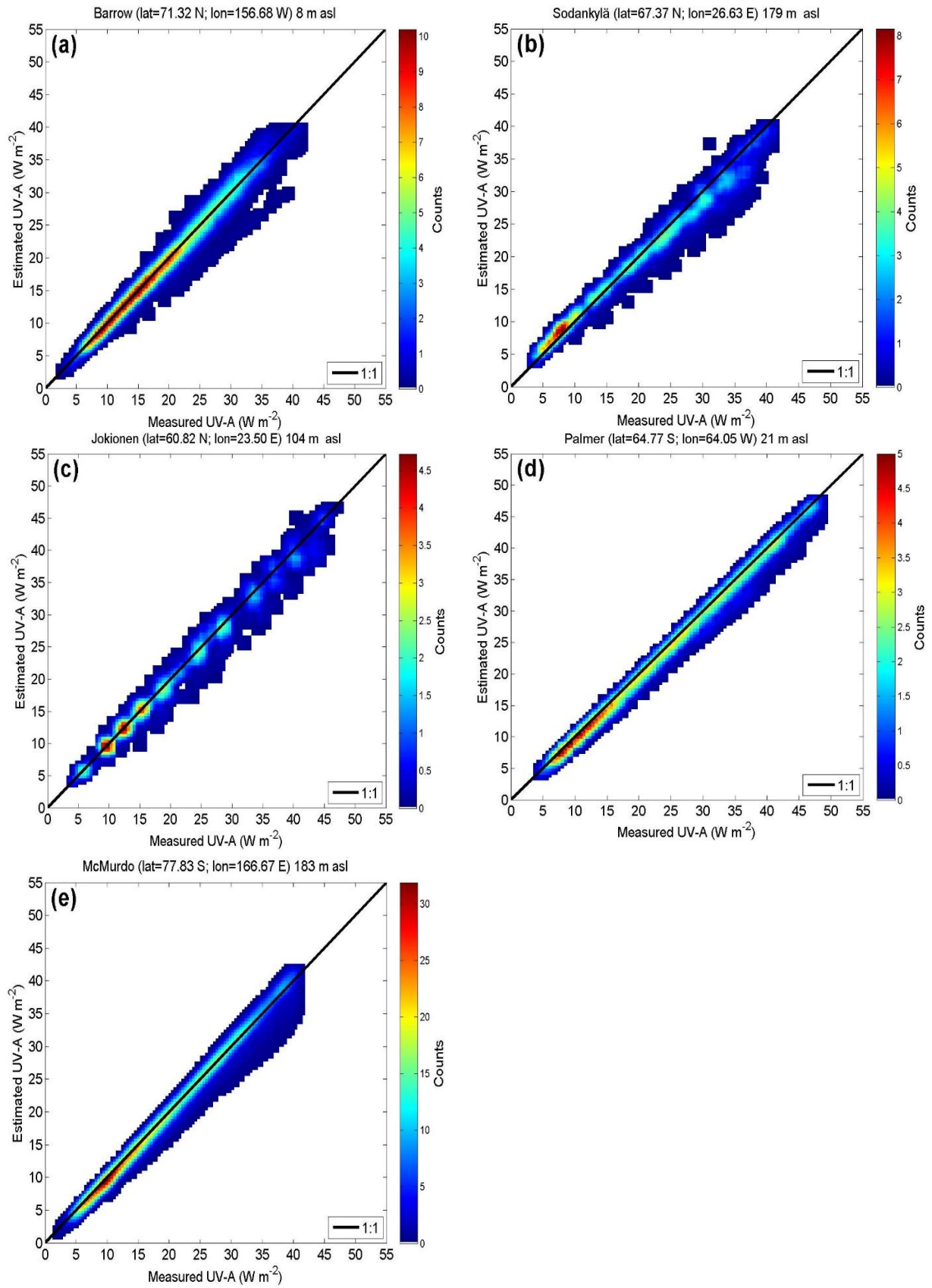
Figure 2: Scatter density plot between measurements of UV−A and estimates for each station with each station name at top. The colorbar indicates the number of points in the area within the interval 0.4 W m^{-2} x 0.4 W m^{-2}
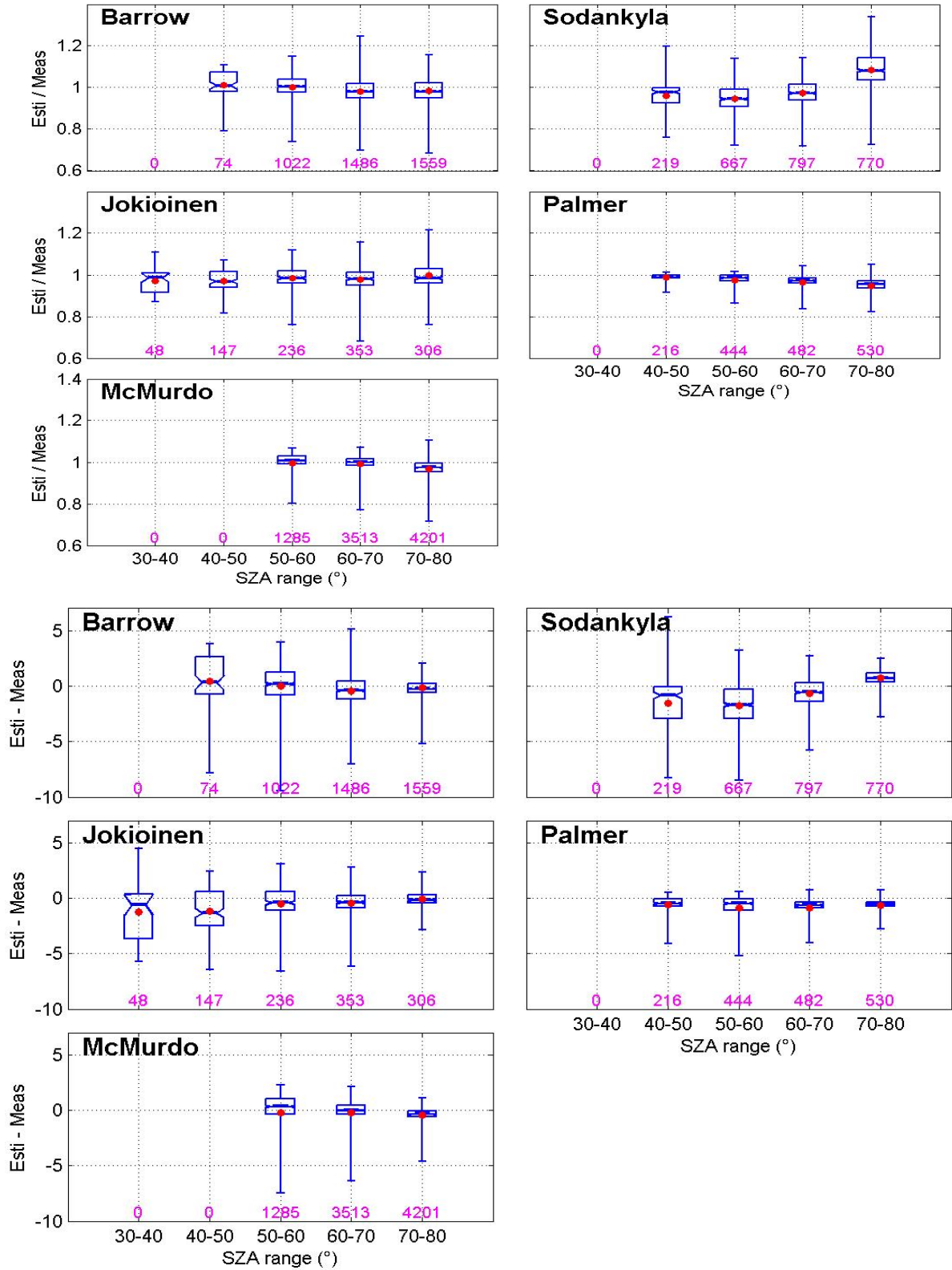
Figure 3: Dependence of ratio (top) of the estimated (Esti) to the measured (Meas) and difference between estimated and measured (bottom) by SZA range for UV−A irradiances for each station. The red dots indicates the mean, the limits of the boxes are 1st, 2nd (median), 3rd quartiles. The lower whisker is the minimum and the upper one is the maximum. The pink number is the number of data in a single SZA range.
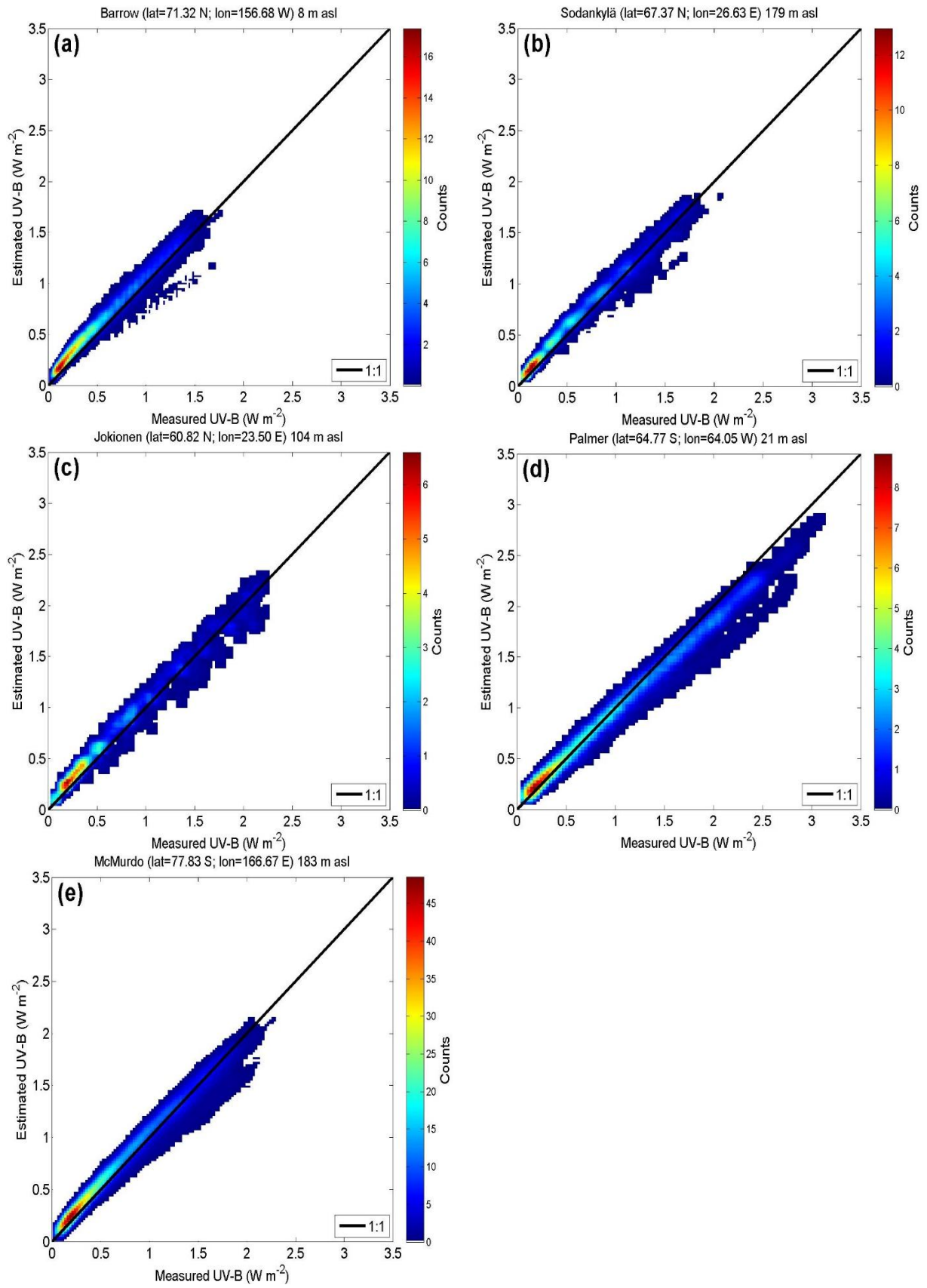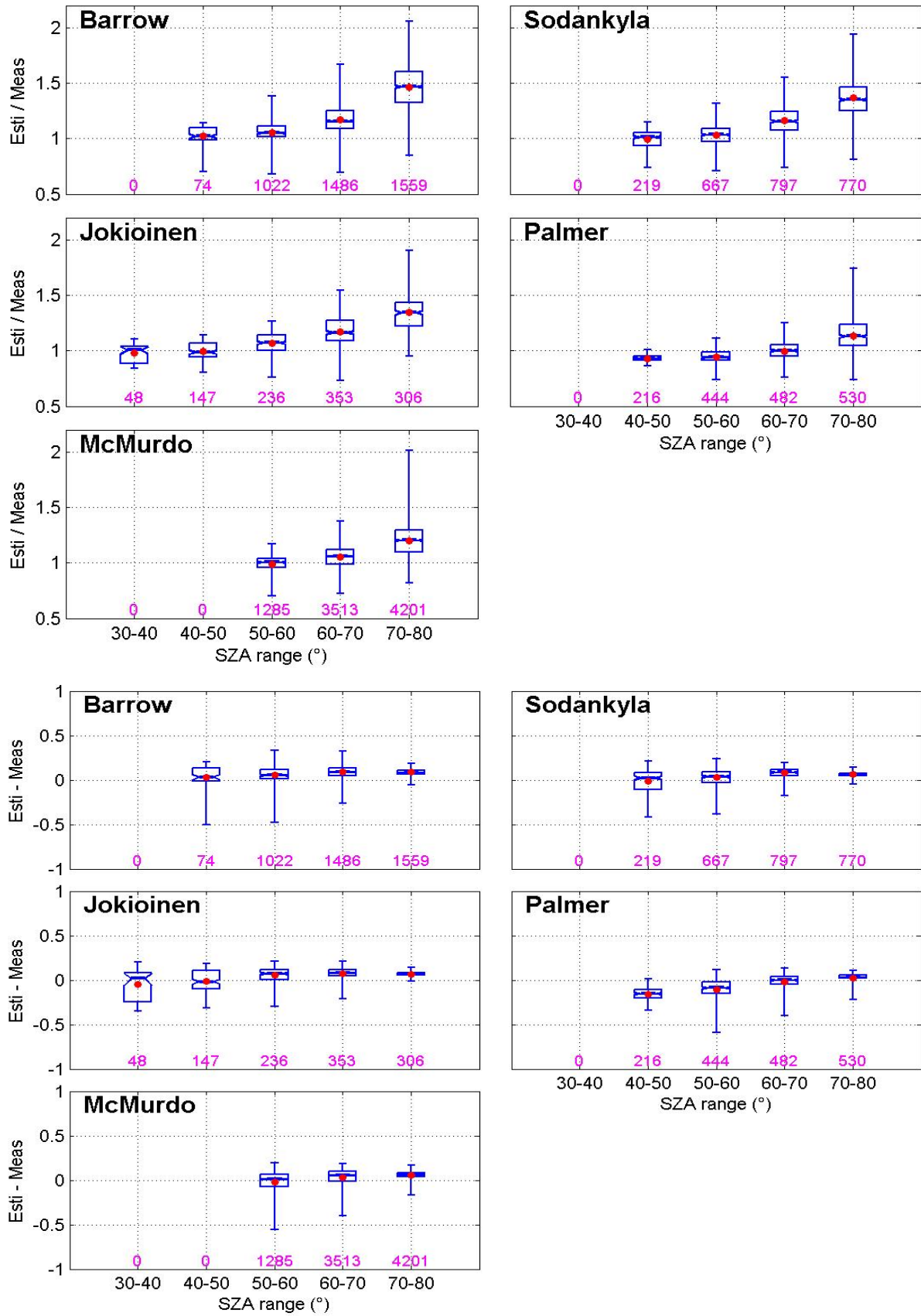
Figure 4: Same as Fig. 2, but for UV–B.

Figure 5: Same as Fig. 3, but for UV–B irradiances.